

Elevated weathering rates in the Rocky Mountains during the Early Eocene Climatic Optimum

M. ELLIOT SMITH^{1*}, ALAN R. CARROLL¹ AND ERICH R. MUELLER²

¹Department of Geology and Geophysics, University of Wisconsin-Madison, 1215 W Dayton St., Madison WI 53706, USA

²Department of Geography, University of Colorado, Boulder, Colorado 80309, USA

*Current address: Department of Geology, Sonoma State University, 1801 E Cotati Ave, Rohnert Park, California 94928, USA

†e-mail: michael.smith@sonoma.edu

Published online: 25 May 2008; doi:10.1038/ngeo205

During the chemical weathering of silicate minerals, atmospheric carbon dioxide is incorporated into carbonate minerals and buried. As the rate of silicate weathering is thought to increase in response to increasing atmospheric CO₂ concentrations, this represents an important negative feedback mechanism¹. Quaternary records of weathering reflect a narrow range of pCO₂ (180–300 p.p.m.v.)²; therefore, the extent of this feedback has been difficult to predict for increasing concentrations of atmospheric CO₂. However, high CO₂ levels of up to 1,125 p.p.m.v. have been suggested for the Early Eocene Climatic Optimum (52 to 50 million years ago)^{3–5}. Here, we combine ⁴⁰Ar/³⁹Ar ages⁶ and the measured volumes of river-derived sediments and sodium-bearing evaporites to determine rates of physical erosion and chemical weathering in the Green River Basin, western United State of America, during the Early Eocene Climatic Optimum⁷. We find physical erosion rates of 420 ± 79 t km² yr⁻¹ and chemical weathering rates of 62.5 ± 21.9 t km² yr⁻¹. The calculated denudation rates of 175 ± 30 m Myr⁻¹ rival the highest documented non-glacial Quaternary rates for crystalline bedrock⁸. We suggest that elevated atmospheric CO₂ levels during the Early Eocene epoch led to enhanced silicate dissolution rates⁹, and thus to increased production of loose rock material and higher rates of physical weathering and denudation.

The Wilkins Peak Member (WPM) of the Eocene Green River Formation was deposited between 51.1 and 49.6 Myr ago in the Greater Green River Basin (GGRB), which was confined by the Sevier fold-and-thrust belt and several antiformal, basement-cored ‘Laramide’ uplifts¹⁰ (Fig. 1, Supplementary Information, Tables S1,S2). The WPM includes ~4,600 km³ of strata deposited in a hydrologically closed basin, and consists predominantly of lacustrine carbonates and subsidiary Na-rich evaporite deposits and horizons of siliciclastic alluvium (Fig. 2a). Evaporites in the WPM constitute the world’s largest commercial soda ash deposit, are comprised primarily of trona (NaHCO₃·Na₂CO₃·2H₂O) and halite (NaCl) and were mapped from over 200 exploratory boreholes¹¹ (see Supplementary Information, Table S3). Detailed stratigraphic analysis of the WPM indicates that the basin was replenished with water and solutes on multiple occasions¹² (Fig. 2). Time-equivalent alluvial facies surround the WPM, filling several sub-basins in the eastern GGRB (refs 13,14) (Fig. 2b). Uplifts to the south, east and north shed ~9,500 km³ of arkosic alluvium

to the basin, whereas uplifts to the south and west contributed ~2,300 km³ of quartz-rich alluvium. Time-equivalent deposits in adjoining basins reflect either internal drainage with accompanying evaporite deposition (Piceance Creek Basin) or external drainage away from the GGRB (ref. 6) (Fig. 1). Six ash horizons dated using the ⁴⁰Ar/³⁹Ar method permit the calculation of accumulation rates for bulk volumes of lacustrine carbonate and alluvium over the 1.5 Myr of WPM deposition, and provide a detailed history of accumulation of Na (ref. 6) (Fig. 2).

The areal extent, bedrock geology, denudation history and climate of the palaeocatchment for the Eocene GGRB are generally well constrained based on regional palaeocurrent, provenance, geochemical and palaeobotanical observations^{6,15}. Uncertainty persists regarding the positions of the eastern and western drainage boundaries of the basin, with the position of the western drainage boundary within the Sevier fold-and-thrust belt the least well constrained (Fig. 1). We estimate an exposed area of Precambrian basement in the GGRB palaeocatchment of 17,900 ± 2,200 km². On a regionally averaged basis, rocks in the cores of uplifts surrounding the GGRB contain 2.6 ± 0.2 wt% Na, 1.7 ± 0.4 wt% Ca and have modal volume proportions of 28 ± 2% quartz and 45 ± 4% plagioclase (see Supplementary Information, Table S1). In contrast, Phanerozoic strata within the catchment contain 0.5 ± 0.2 wt% Na, 3.1 ± 1.8 wt% Ca and are arkosic to quartz arenitic in composition^{16,17}. Late Palaeozoic halite-bearing strata occur atop the White River–Sawatch uplift trend in northwest Colorado, but were not unroofed and exposed to weathering before their burial by Oligocene basalt flows, and occur south of the drainage divide for the GGRB¹⁸ (Fig. 1). Palaeogene syn-orogenic strata deposited before the WPM are arkosic to quartzose in composition, but most would have been sequestered in actively subsiding Laramide basins during WPM time¹⁵. Owing to widespread Cenozoic erosion, the lithologies exposed atop basement uplifts during the Early Eocene are known only from sediments shed from them into adjacent basins. Conglomeratic proximal deposits exhibit unroofing sequences indicative of ongoing denudation of the Phanerozoic cover and underlying crystalline basement during the ~11 Myr from the Middle Palaeocene to Early Eocene epoch¹⁵, consistent with fission-track thermochronology indicating concurrent denudation rates between 130 and 350 m Myr⁻¹ for basement uplifts¹⁹. In the GGRB, net sediment accumulation rates of 100–300 m Myr⁻¹ throughout the Eocene imply ongoing burial

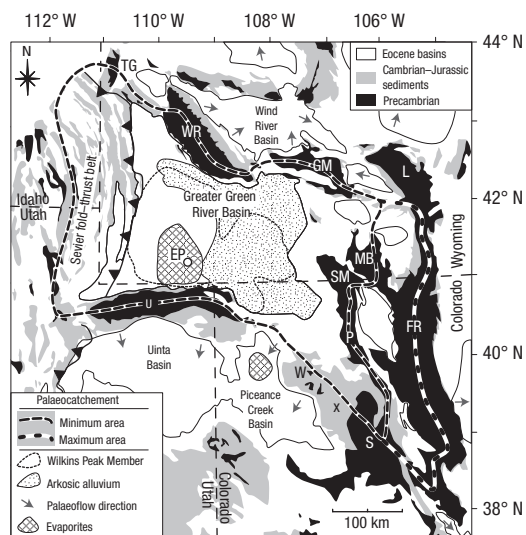


Figure 1 Map of the central Rocky Mountain lake province showing the Early Eocene palaeocatchment of the GGRB⁸. X: Pennsylvanian–Permian Eagle Valley evaporite; EP: El Paso 44–3 core; TG: Teton–Gros Ventre uplift; WR: Wind River uplift; GM: Granite Mountains uplift; L: Laramie uplift; MB: Medicine Bow uplift; SM: Sierra Madre uplift; P: Park–Gore uplift; FR: Front Range uplift; W: White River uplift; S: Sawatch uplift.

of the resulting detritus⁶. Leaf fossils from the WPM indicate a dry subtropical climate with mean annual rainfall of $\sim 80 \text{ cm yr}^{-1}$ and average annual temperatures of $\sim 20^\circ \text{C}$ (ref. 20).

We seek to compare Early Eocene chemical weathering and physical erosion with Quaternary processes and rates. We consider several types of data: (1) chemical and physical sediment volumes (Fig. 2, Supplementary Information, Tables S2,S3), (2) radioisotopic ages for ash beds⁶ and (3) the chemistry and modal mineralogy of crystalline basement and basinal strata (see Supplementary Information, Tables S1,S2). Total and element-specific chemical depletion fractions⁸ (CDFs) are used to denote the relative proportion of chemical weathering to total denudation. Subscripts are used to indicate the element-specific CDF values (CDF_{Na}), or to indicate a method of determination (CDF_{D} and CDF_{S} ; see Table 1). Uncertainties for all calculations were fully propagated and are given at the 1σ level throughout²¹ (see the Methods section for more details).

Approximately $1.54 \times 10^{14} \text{ t}$ of arkosic alluvium occupies the eastern GGRB (Fig. 2a), providing a direct measure of bulk physical erosion in the eastern GGRB catchment. However, erosional flux from crystalline bedrock (E) cannot be precisely determined without knowledge of the fraction that was derived from erosion of Phanerozoic strata (PhF). Crystalline bedrock is currently exposed across $\sim 80\%$ of the structural uplifts in the eastern catchment area, and basin-margin conglomerate clast compositions indicate removal of Phanerozoic cover from most uplift crests by the Early Eocene¹⁵. Nonetheless, Phanerozoic rocks are more easily eroded than crystalline basement, and probably contributed disproportionately to the clastic sediment flux relative to their exposed area. Crystalline rocks in the eastern catchment have a plagioclase to quartz ratio of 1.6 ± 0.5 ($n = 175$, see Supplementary Information, Table S1), whereas this ratio drops to 0.6 ± 0.2 in very fine to coarse-grained sandstones in the lower WPM and time-equivalent arkosic alluvium (Fig. 2d). This decrease is attributable to two independent processes: (1) *in situ* chemical dissolution of plagioclase before erosion and transport, which is directly proportional to the Na depletion fraction

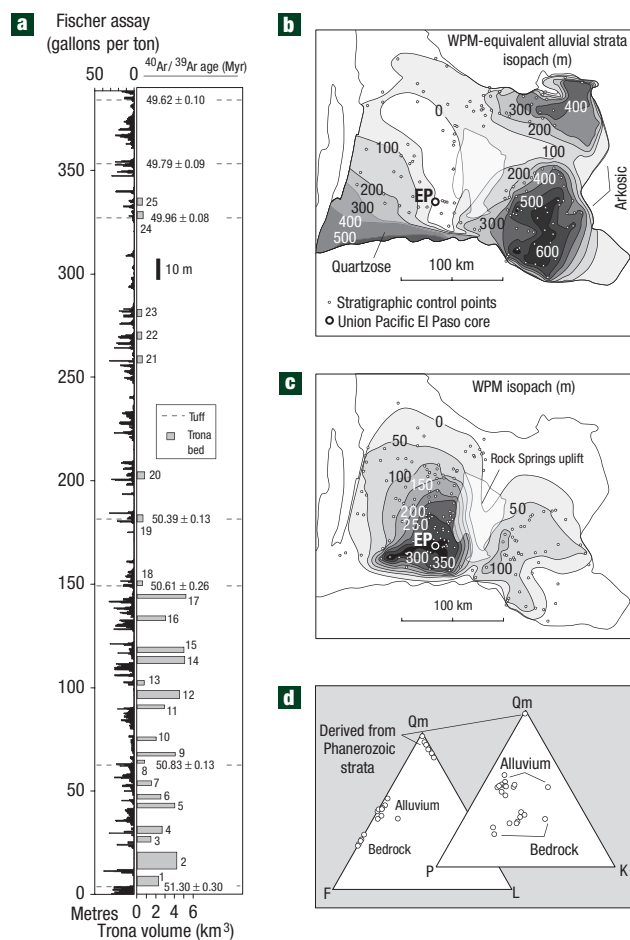


Figure 2 Early Eocene strata in the GGRB. **a**, Stratigraphy of the WPM in the Union Pacific El Paso 44–3 core³⁰, which penetrated the entire Green River Formation; ages shown with 2σ uncertainties; Fischer assay maxima correspond to periods of lake expansion¹². Isopachs interpolated from published stratigraphy using the natural-neighbour method in ArcGIS (see Supplementary Information, Table S2). **b**, WPM. **c**, Time-equivalent alluvial strata. **d**, Sandstone compositional modes for crystalline basement and basinal alluvium (see Supplementary Information, Table S1). Each sandstone sample was counted at 400 grid locations. Qm: monocrystalline quartz; F: feldspar; L: lithic fragments; K: K-feldspar; P: plagioclase.

(CDF_{Na}) because virtually all Na occurs in plagioclase; and (2) the admixture of quartz derived from erosion of Phanerozoic strata, which is directly proportional to PhF.

To calculate chemical weathering rates for crystalline bedrock, Ca and Na solute fluxes to the GGRB were determined from volumes of chemical sediment and $^{40}\text{Ar}/^{39}\text{Ar}$ ages for ash beds. The WPM contains approximately $1.00 \times 10^{13} \text{ t}$ of lacustrine strata containing $11 \pm 5 \text{ wt}\%$ Ca (ref. 22) (Fig. 2b). Assuming Ca was derived from both atmospheric deposition (modern local deposition = $0.12 \pm 0.01 \text{ t km}^{-2} \text{ yr}^{-1}$) (ref. 23) and chemical weathering across a catchment that includes an imprecisely known area of the Sevier fold-and-thrust belt, we calculate an imprecise average Ca weathering flux of $16 \pm 11 \text{ t km}^{-2} \text{ yr}^{-1}$. Because Phanerozoic strata contain nearly twice as much Ca as crystalline bedrock, and their Eocene areal extent is poorly constrained, a Ca weathering flux from crystalline bedrock cannot be confidently differentiated from zero. Na in WPM evaporites provides a more precise constraint on chemical weathering fluxes because crystalline

Table 1 Physical erosion, chemical weathering and denudation rates. (All values are for crystalline bedrock in the GGRB catchment. Uncertainties are expressed at 1 σ level (see the Methods section for details); preferred rates were calculated by solving for $CDF_D = CDF_S$, and are shown in bold.)

PhF*	$\Delta E_{P/C}$ †	E ‡ ($t\text{ km}^{-2}\text{ yr}^{-1}$)	W § ($t\text{ km}^{-2}\text{ yr}^{-1}$)	D_S ¶ ($m\text{ Myr}^{-1}$)	CDF_S ††	CDF_{Na}^{**}	CDF_D ††	D_{Na} †† ($m\text{ Myr}^{-1}$)
0.200	1.0	605 ± 114	60.1 ± 21.8	242 ± 42	0.09 ± 0.04	0.50 ± 0.07	0.23 ± 0.04	89 ± 35
0.300	1.7	530 ± 100	60.1 ± 21.8	214 ± 37	0.10 ± 0.04	0.43 ± 0.06	0.20 ± 0.04	104 ± 41
0.400	2.7	454 ± 86	61.4 ± 21.8	187 ± 32	0.12 ± 0.05	0.33 ± 0.04	0.16 ± 0.03	137 ± 54
0.445	3.2	420 ± 79	62.5 ± 21.9	175 ± 30	0.13 ± 0.05	0.28 ± 0.04	0.13 ± 0.02	167 ± 66
0.500	4.0	378 ± 71	64.5 ± 22.0	161 ± 27	0.15 ± 0.06	0.20 ± 0.03	0.09 ± 0.02	242 ± 95
0.550	4.9	341 ± 64	67.0 ± 22.4	148 ± 25	0.16 ± 0.06	0.11 ± 0.01	0.05 ± 0.01	462 ± 182

*Proportion of WPM-equivalent alluvium in the eastern GGRB derived from erosion of Phanerozoic strata.

† Differential physical erosion rates for Phanerozoic strata versus crystalline bedrock, assuming crystalline rock was exposed across 80% of uplifts in the eastern catchment.

‡ Physical erosion rate for crystalline basement in the eastern GGRB catchment, calculated by removing PhF from the total clastic sediment flux.

§ Chemical weathering rate for crystalline basement in the GGRB, calculated by multiplying the Na weathering flux from crystalline bedrock (W_{Na} : $3.69 \pm 0.94\text{ t km}^{-2}\text{ yr}^{-1}$) by a [total solutes]/Na conversion factor of 19.0 ± 1.6 . This value represents the weighted average of the proportion of total solutes to Na leached from regolith at 42 sites on crystalline bedrock, calculated from bedrock and soil compositions⁸. Individual [total solutes]/Na values for modern sites⁸ were scaled to correct for the difference in Na wt% relative to crystalline bedrock in the GGRB palaeocatchment (see Supplementary Information, Table S1). W_{Na} was corrected for both atmospheric deposition and contributions from the weathering of Phanerozoic bedrock (see the Methods section).

¶ Denudation rate derived from addition of W and E (see the Methods section).

†† The proportion of W to D_{Na} (see the Methods section).

**Proportion of Na removed from regolith before transport and deposition. Calculated from modal proportions of plagioclase and quartz in basinal alluvial and crystalline bedrock in the GGRB catchment, and assuming that all Na in crystalline basement is contained in plagioclase (see the Methods section).

††† Calculated from CDF_{Na} using CDF/CDF_{Na} conversion factor (0.47 ± 0.13) derived from robust linear regression of overall CDF versus CDF_{Na} values at 42 sites on crystalline bedrock in a wide spectrum of climatic conditions⁸.

‡‡ Denudation rate for crystalline rocks in the GGRB, calculated from W_{Na} and CDF_{Na} determined from PhF, assuming a regolith profile of constant thickness was continually forming via partial chemical decomposition (equivalent to CDF_{Na}) and physically eroded in a steady-state fashion (see the Methods section).

bedrock contains more than five times more Na than Phanerozoic strata. Mapped trona beds contain $\sim 4.1 \times 10^{10}$ tonnes of Na, probably an underestimate due to numerous unmapped thin trona horizons, widely disseminated shortite ($\text{Na}_2\text{CO}_3 \cdot 2\text{CaCO}_3$) and >50% halite in several evaporite beds¹¹. Approximately 93% of Na occurs in the lower half of the WPM, where evaporite beds are regularly associated with the regressive stages of individual lacustrine expansion–contraction cycles. The upper WPM contains relatively little Na (ref. 12) (Fig. 2, Supplementary Information, Table S3). We interpret the upsection decline in Na accumulation to reflect a hydrologic shift that permitted solute-bearing waters to intermittently overflow the sill of the GGRB into the Piceance Creek Basin, where evaporite deposition continued for a further 1.5 Myr (ref. 6). ⁴⁰Ar/³⁹Ar ages for ashes bounding the lower WPM yield a Na accumulation rate of $73,200 \pm 15,100\text{ t yr}^{-1}$. The majority of this flux (70–84%) was derived from weathering of crystalline bedrock (W_{Na}), with the remainder attributable to atmospheric deposition and chemical weathering of Phanerozoic strata. Assuming Eocene atmospheric deposition across the GGRB catchment was similar to modern rates ($0.052 \pm 0.004\text{ t km}^{-2}\text{ yr}^{-1}$) (ref. 23), and zero net loss from the basin due to wind deflation, atmospheric Na represents 10% of the total Na flux. The quantity of Na derived from the chemical weathering of Phanerozoic rocks varies from 4–13% of the total Na with different plausible PhF values. Subtracting atmospheric and Phanerozoic-derived Na from the total Na accumulation yields W_{Na} values between 3.2 and $3.5\text{ t km}^{-2}\text{ yr}^{-1}$. We convert this to a total solute flux (W) by applying a [total solute]/Na conversion factor of 19.0 ± 1.6 estimated from chemical compositions of weathered regolith and crystalline bedrock in modern soil profiles at 42 locations encompassing a spectrum of climates and denudation rates⁸ (Table 1).

Because of the influence of PhF on both E and W calculations, mass-balance calculations were carried out to examine the effects of a range of PhF values. Two independent methods for calculating total denudation (D) were used, and a PhF of 0.445 was determined to be the most mutually consistent solution to this multicomponent mixing problem (Table 1, Supplementary Information, Fig. S1). At this value, $E = 420 \pm 79\text{ t km}^{-2}\text{ yr}^{-1}$, $W = 62.5 \pm 21.9\text{ t km}^{-2}\text{ yr}^{-1}$ and $D_S = 175 \pm 30\text{ m Myr}^{-1}$, which we consider the most accurate estimates for these rates during the 1.5 Myr of WPM deposition.

These values are largely insensitive to the exposed Eocene area of crystalline bedrock, and imply that Phanerozoic strata were eroded ~ 3.2 times faster than basement rocks. Calculated rates occurred across at least $\sim 17,900\text{ km}^2$ and imply $266 \pm 46\text{ m}$ of denudation from basement uplifts during WPM deposition. We argue that this 200–300 m of lowering is unlikely to result from a simple flushing of pre-existing regolith, given that typical regolith is one to tens of metres thick. It requires instead significant propagation of a weathering front to generate new regolith, which is subsequently transported to the basins. Although closed-basin-based denudation records for other periods of the Palaeogene have yet to be documented, similar rates of denudation were plausibly ongoing throughout given the similar climatic conditions and thick packages of syn-orogenic strata in many Laramide basins^{10,20}. These rates are an order of magnitude faster than most Quaternary rates for non-glacial catchments underlain by resistant lithologies, and are matched only by sediment-flux-based rates in a few small catchments ($< 1,000\text{ km}^2$) and by cosmogenically derived rates from ridge tops and hillslopes with gradients $> 0.45\text{ m/m}$ (ref. 8) (Fig. 3).

The fastest documented modern and Quaternary chemical weathering rates do not coincide with the hottest, wettest climates because heavy vegetation inhibits erosion (Fig. 3), but instead occur in high-relief regions, where physical erosion prevents regolith from building up on slopes, allowing propagation of the weathering front into fresh bedrock. Sediment yields from such ‘weathering-limited’ landscapes indicate that weathering reaction rates are well correlated with rainfall and temperature^{8,9}. In contrast, the effects of atmospheric $p\text{CO}_2$ on weathering rates are less well understood. In one experiment, increased atmospheric $p\text{CO}_2$ led to enhanced plant growth and root respiration, which resulted in increased soil $p\text{CO}_2$ and chemical weathering rates²⁴, suggesting that higher $p\text{CO}_2$ during the Early Eocene³ may explain W rates of 4.4 ± 1.4 times faster than the average values for weathering-limited modern catchments $> 1,000\text{ km}^2$ with similar climates (see the Methods section). We propose that rapid W resulting from Early Eocene $p\text{CO}_2$ (ref. 3) and the ongoing uplift and denudation of Laramide basement structures promoted the observed high denudation rates, and expect that similar weathering and denudation rates may have occurred during other periods of Earth history characterized by elevated $p\text{CO}_2$.

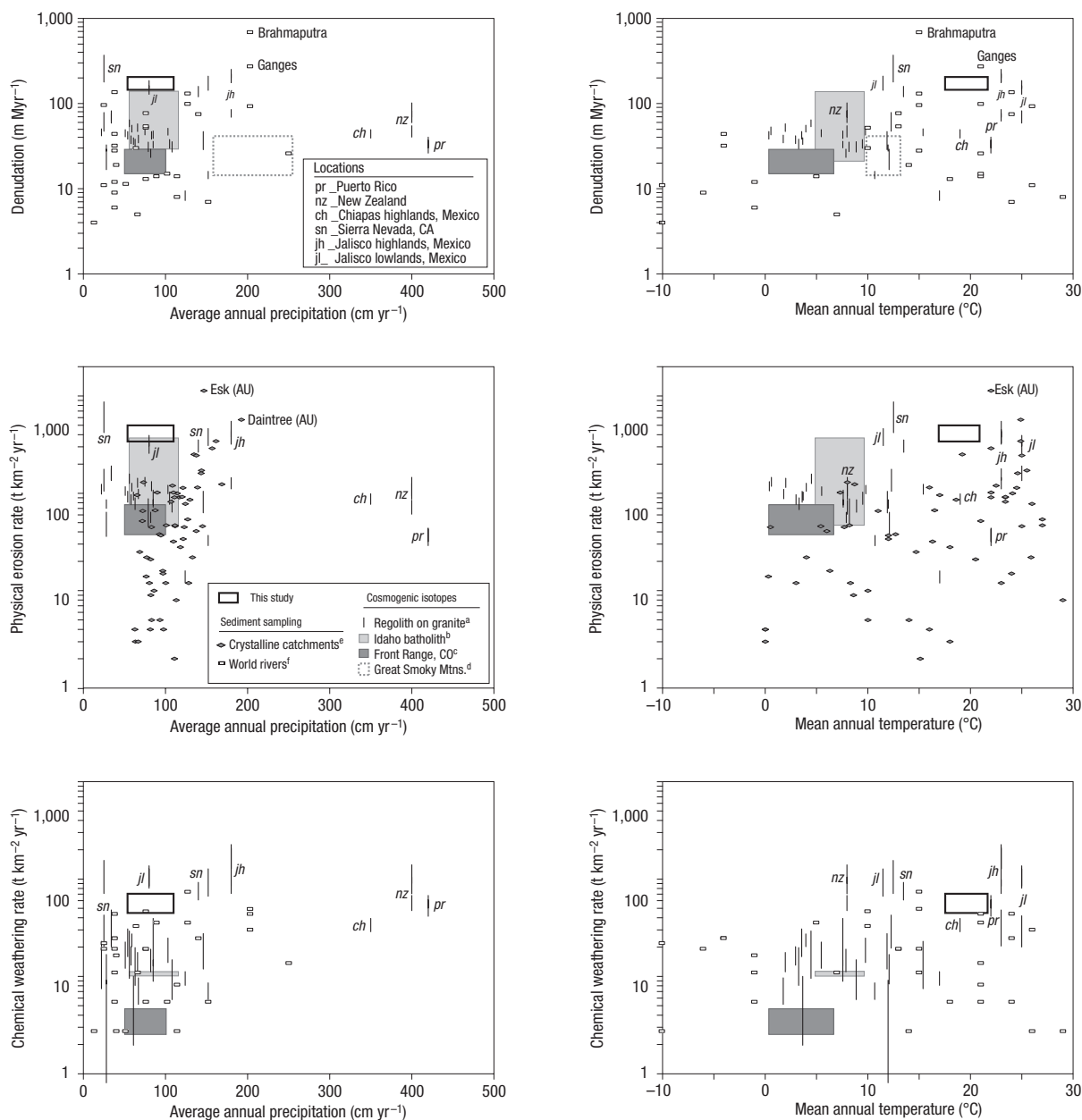


Figure 3 Comparison of Eocene chemical weathering, physical erosion and overall denudation rates to Quaternary rates for unglaciated granitic catchments. Taken from three sources: (1) contemporary river sediment and solute discharge measurements^{25,28}, (2) modelled from cosmogenic nuclide concentrations in river sediments^{26,27,29} or (3) modelled from cosmogenic nuclides in regolith and bulk chemistry of regolith and bedrock⁸. Rates are plotted relative to average annual rainfall (left) and mean annual temperature (right) derived from leaf fossils, and shown with 1σ uncertainties²⁰.

METHODS

CALCULATION OF UNCERTAINTIES

Uncertainties were determined by quadratically propagating the uncertainties associated with the individual components of each calculated value, with the assumption that errors are not correlated²¹. Individual 1σ uncertainties were either taken from reported values, or calculated as follows: (A) in cases where variance in the measurement of a given quantity is a function of sampling or analytical errors alone, we use the standard error of the mean (s.e.); (B) in cases where uncertainties are reported for the values used to calculate a given quantity, a weighted-mean calculation was applied, in which the resulting uncertainty was multiplied by the square root of the MSWD (mean square of weighted deviates) when MSWD > 1; (C) if the variance in measurements of a given quantity is a function of heterogeneity of the sampled materials, we use

the standard deviation (s.d.); (D) if uncertainty could not be calculated directly from statistical dispersion, uncertainty was estimated on the basis of known constraints; and (E) where maximum and minimum values for a quantity are constrained, we take the difference between the maximum and average value to indicate 1σ uncertainty. The method of uncertainty determination for specific quantities is indicated below with lettered superscripts.

EMPIRICAL CONSTRAINTS

Rates were calculated using the following suite of empirical constraints and associated uncertainties. Lacustrine strata (see Supplementary Information, Table S2): volume (V_L)^D = 4,630 ± 463 km³, density (ρ_L) = 2.20, composition (C_{L-Ca}) (ref. 22) = 10.75 ± 4.57 wt% Ca^C. WPM evaporites (see Supplementary Information, Table S3): V_E^D = 56.1 ± 2.8 km³ (WPM total), V_E^D = 52.3 ± 2.6 km³ (lower WPM), ρ_E = 2.13¹⁰, composition (C_{E-Na}) = 36.3 ± 0.5 wt% Na

(ref. 11). WPM-equivalent alluvium (eastern GGRB): $V_{Ac} = 9,509 \pm 951 \text{ km}^3 \text{ D}$, $\rho_A = 2.16$, modal mineralogy (MM_{Ac-Q}) = $51.2 \pm 3.4\%$ quartz^C, $MM_{Ac-P} = 33.2 \pm 7.8\%$ plagioclase^C. WPM-equivalent alluvium (western GGRB): $V_{Aw} = 2,300 \pm 230 \text{ km}^3 \text{ D}$, $\rho_A = 2.16$, $MM_{Aw-Q} = >97\%$ quartz^C. Precambrian crystalline basement (see Supplementary Information, Table S1): areal extent (AE_C) = $17,860 \pm 2,170 \text{ km}^2 \text{ E}$, $\rho_C = 2.75$, $C_{C-Na} = 2.60 \pm 0.48 \text{ wt\% Na}^C$, $C_{C-Ca} = 1.68 \pm 1.17 \text{ wt\% Ca}^C$, $MM_{C-Q} = 25.4 \pm 1.8\%$ quartz^C, $MM_{C-P} = 44.0 \pm 3.7\%$ plagioclase^C. Phanerozoic strata¹⁶: $AE_{Ph} = 42,860 \pm 20,000 \text{ km}^2 \text{ E}$, $\rho_{Ph} = 2.16$, $C_{Ph-Na} = 0.52 \pm 0.17 \text{ wt\% Na}^C$, $C_{Ph-Ca} = 3.09 \pm 1.79 \text{ wt\% Ca}^C$. GGRB palaeocatchment⁶: $AE_G = 140,000 \pm 14,000 \text{ km}^2 \text{ E}$. Modern atmospheric deposition²³: $At_{Na} = 0.052 \pm 0.004 \text{ t km}^{-2} \text{ yr}^{-1} \text{ A}$, $At_{Ca} = 0.121 \pm 0.010 \text{ t km}^{-2} \text{ yr}^{-1} \text{ A}$. Duration⁶: WPM (δt_{WPM}) = $1.52 \pm 0.16 \text{ Myr}$, lower WPM (δt_{WPl}) = $0.55 \pm 0.16 \text{ Myr}$. [Total solutes]/Na (ref. 8): 19.0 ± 1.6^B . [CDF/CDF_{Na}] (ref. 8): 0.47 ± 0.13^A . Palaeobotanically determined palaeoclimate²⁰: mean annual temperature = $19.6 \pm 2.1^\circ \text{C}$. Average annual rainfall = $76.9 + 33.2 / -23.2 \text{ cm yr}^{-1}$. Average rates for modern crystalline catchments $>1,000 \text{ km}^2$ with mean annual temperature = $15\text{--}29^\circ \text{C}$ and average annual rainfall = $60\text{--}14 \text{ cm yr}^{-1}$: $E_M = 77.5 \pm 70.2 \text{ t km}^{-2} \text{ yr}^{-1} \text{ C}$ ($n = 40$ (refs 25–28)), $W_M = 10.3 \pm 6.5 \text{ t km}^{-2} \text{ yr}^{-1} \text{ C}$ ($n = 7$ (refs 26–28)), $D_M = 48.3 \pm 33.7 \text{ m Myr}^{-1} \text{ C}$ ($n = 11$ (refs 25–29)).

CALCULATED VALUES

The following equations were used in cited calculations. (1) Physical erosion rate from crystalline bedrock: $E = V_{Ac} \cdot (1 - \text{PhF}) / \delta t_{WPM}$. (2) Na weathering flux from Phanerozoic strata: $W_{Ph-Na} = ((V_{Ac} \cdot (\Delta E_{P/C} \cdot 0.2) / ((\Delta E_{P/C} \cdot 0.2) + 0.8) + W_{Aw}) \cdot \text{CDF}_{Na} \cdot C_{Ph-Na}) / (1 - \text{CDF}_D)$. (3) Atmospheric Na flux to GGRB: $F_{Na-atm} = At_{Na} \cdot AE_G$. (4) Atmospheric Ca flux to GGRB: $F_{Ca-atm} = At_{Ca} \cdot AE_G$. (5) Na weathering flux from crystalline bedrock: $W_{Na} = (V_{El} \cdot \rho_E \cdot C_{E-Na}) - (F_{Na-atm} + W_{NaPh})$. (6) Ca weathering flux from entire catchment: $W_{Ca} = (V_L \cdot \rho_L \cdot C_{L-Ca}) - (F_{Ca-atm})$. (7) Total weathering flux from crystalline bedrock: $W = W_{Na} \cdot [\text{total solutes}] / Na$. (8) Denudation rate from clastic and chemical sediment volumes: $D_S = E + W$. (9) Chemical depletion fraction from clastic and chemical sediment volumes: $\text{CDF}_S = W / D_S$. (10) Na depletion fraction for crystalline bedrock: $\text{CDF}_{Na} = 1 - ((MM_{Ac-P} / ((MM_{Ac-Q} \cdot (1 - \text{PhF})) / MM_{C-Q})) / MM_{C-P})$. (11) Denudation rate calculated from CDF_{Na} by assuming steady-state erosion of a regolith profile of constant thickness and Na depletion = CDF_{Na} : $D_{Na} = W_{Na} / (\rho_C \cdot C_{C-Na} \cdot \text{CDF}_{Na})$. (12) Chemical depletion fraction associated with D_{Na} : $\text{CDF}_D = \text{CDF}_{Na} \cdot [\text{CDF} / \text{CDF}_{Na}]$. (13) Ratio between erosion rates for Phanerozoic strata versus crystalline bedrock, assuming 80% of area of erosion underlain by crystalline rock: $\Delta E_{P/C} = 4 \cdot \text{PhF} / (1 - \text{PhF})$.

FACTORS INFLUENCING MASS-BALANCE CALCULATION

To determine a solution to the multicomponent mixing problem posed by PhF, denudation was calculated using equations (8) and (11) for a range of possible values. D_S is inversely correlated with PhF due to decrease in E with higher PhF, resulting in a higher apparent sediment-derived chemical depletion fraction (CDF_S) because W is essentially unchanged by the correction for Na derived from weathering of Phanerozoic strata. Conversely, D_{Na} is positively correlated to PhF due to decreases in plagioclase decomposition required to obtain the observed modal proportion of plagioclase in basinal detritus (indicated by CDF_{Na}), increasing the bedrock to regolith conversion rate necessary to produce the observed W_{Na} .

Received 4 February 2008; accepted 22 April 2008; published 25 May 2008.

References

- Suchet, P. A. & Probst, J. L. A global model for present-day atmospheric/soil CO₂ consumption by chemical erosion of continental rocks (GEM-CO₂). *Tellus B* **47**, 273–280 (1995).
- Petit, J. R. *et al.* Climate and atmospheric history of the past 420,000 years from the Vostok ice core, Antarctica. *Nature* **399**, 429–436 (1999).

- Lowenstein, T. K. & Demicco, R. V. Elevated Eocene atmospheric CO₂ and its subsequent decline. *Science* **313**, 1928 (2007).
- Zachos, J., Pagani, M., Sloan, L., Thomas, E. & Billups, K. Trends, rhythms, and aberrations in global climate 65 Ma to present. *Science* **292**, 685–693 (2001).
- Fletcher, B. J., Brentnall, S. J., Anderson, C. W., Berner, R. A. & Beerling, D. J. Atmospheric carbon dioxide linked with Mesozoic and early Cenozoic climate change. *Nature Geosci.* **1**, 43–48 (2008).
- Smith, M. E., Carroll, A. R. & Singer, B. S. Synoptic reconstruction of a major ancient lake system: Eocene Green River Formation, Western United States. *Geol. Soc. Am. Bull.* **120**, 54–84 (2008).
- Einsle, G. & Hinderer, M. Quantifying denudation and sediment-accumulation systems (open and closed lakes): Basic concepts and first results. *Palaeogeogr. Palaeoclimatol. Palaeoecol.* **140**, 7–21 (1998).
- Riebe, C. S., Kirchner, J. W. & Finkel, R. C. Erosional and climatic effects on long-term chemical weathering rates in granitic landscapes spanning diverse climate regimes. *Earth Planet. Sci. Lett.* **224**, 547–562 (2004).
- West, A. J., Galy, A. & Bickle, M. Tectonic and climatic controls on silicate weathering. *Earth Planet. Sci. Lett.* **235**, 211–228 (2005).
- Dickinson, W. R. *et al.* Paleogeographic and paleotectonic setting of Laramide sedimentary basins in the central Rocky Mountain region. *Geol. Soc. Am. Bull.* **100**, 1023–1039 (1988).
- Wiig, S. V., Grundy, W. D. & Dyni, J. R. Trona resources in the Green River Basin, southwest Wyoming. US Geological Survey Open-File Report OF 95-476 (1995).
- Pietras, J. T. & Carroll, A. R. High-resolution stratigraphy of an underfilled lake basin: Wilkins Peak Member, Eocene Green River Formation, Wyoming, USA. *J. Sedim. Res.* **76**, 1197–1214 (2006).
- Bradley, W. H. The geology of the Green River Formation and associated Eocene rocks in southwestern Wyoming and adjacent parts of Colorado and Utah. US Geological Survey Professional Paper 496-A (1964).
- Roehler, H. W. Description and correlation of Eocene rocks in stratigraphic reference sections for the Green River and Washakie Basins, southwest Wyoming. US Geological Survey Professional Paper 1506-D (1992).
- Carroll, A. R., Chetel, L. M. & Smith, M. E. Feast to famine: Sediment supply control on Laramide basin fill. *Geology* **34**, 197–200 (2006).
- Cullers, R. L. The controls on the major- and trace-element evolution of shales, siltstones and sandstones of Ordovician to Tertiary age in the Wet Mountains region, Colorado, U.S.A. *Chem. Geol.* **123**, 107–131 (1995).
- Hansen, W. R. Geology of the Flaming Gorge area Utah–Colorado–Wyoming. US Geological Survey Professional Paper 490 (1965).
- Kunk, M. J. *et al.* ⁴⁰Ar/³⁹Ar ages of late Cenozoic volcanic rocks within and around the Carbonate and Eagle collapse centers, Colorado; constraints on the timing of evaporite-related collapse and incision of the Colorado River. Geological Society of America Special Paper 366, 213–234 (2002).
- Kelley, S. A. & Chapin, C. E. Denudation history and internal structure of the Front Range and Wet Mountains, Colorado, based on apatite-fission-track thermochronology. New Mexico Bureau of Geology and Mineral Resources Bulletin 160, 41–77 (2004).
- Wilf, P. Late Paleocene–early Eocene climate changes in southwestern Wyoming: Paleobotanical analysis. *Geol. Soc. Am. Bull.* **112**, 292–307 (2000).
- Taylor, J. R. *An Introduction to Error Analysis* (Univ. Science Books, Mill Valley, 1982).
- Mason, G. M. *Mineralogical Aspects of Stratigraphy and Geochemistry of the Green River Formation*, Wyoming. Thesis, Univ. of Wyoming, Laramie (1987).
- Sueker, J. K., Clow, D. W., Ryan, J. N. & Jarrett, R. D. Effect of basin physical characteristics on solute fluxes in nine alpine/subalpine basins, Colorado, USA. *Hydro. Process.* **15**, 2759–2769 (2001).
- Andrews, J. A. & Schlesinger, W. H. Soil CO₂ dynamics, acidification, and chemical weathering in a temperate forest with experimental CO₂ enrichment. *Glob. Biogeochem. Cycles* **15**, 149–162 (2001).
- Syvitski, J. P. M. & Milliman, J. D. Geology, geography, and humans battle for dominance over the delivery of fluvial sediment to the coastal ocean. *J. Geol.* **115**, 1–19 (2007).
- Kirchner, J. W. *et al.* Mountain erosion over 10 yr, 10 k.y., and 10 m.y. time scales. *Geology* **29**, 591–594 (2001).
- Dethier, D. P. & Lazarus, E. D. Geomorphic inferences from regolith thickness, chemical denudation and CRN erosion rates near the glacial limit, Boulder Creek catchment and vicinity, Colorado. *Geomorphology* **75**, 384–399 (2006).
- Summerfield, M. A. & Hulton, N. J. Natural controls of fluvial denudation rates in major world drainage basins. *J. Geophys. Res.* **99**, 871–883 (1994).
- Matmon, A. *et al.* Temporally and spatially uniform rates of erosion in the southern Appalachian Great Smoky Mountains. *Geology* **31**, 155–158 (2003).
- Roehler, H. W. Chart showing identification of oil-shale and trona beds and their geophysical log responses in the Union Pacific Railroad Company El Paso corehole no. 44-3, Eocene Green River Formation, southwest Wyoming. US Geological Survey Miscellaneous Field Studies Map MF-2188 (1991).

Supplementary Information accompanies this paper on www.nature.com/naturegeoscience.

Acknowledgements

We thank B. S. Singer, J. R. Dyni, J. C. Knox, D. C. Kelly, B. Tikoff and J. P. Smoot for assistance or discussions, and appreciate the thoughtful review by R.S. Anderson. Financial support was provided by National Science Foundation grants EAR-0230123, EAR-0114055 and EAR-0516760, and the Bailey Distinguished Graduate Fellowship at the University of Wisconsin.

Author information

Reprints and permission information is available online at <http://npg.nature.com/reprintsandpermissions>. Correspondence and requests for materials should be addressed to M.E.S.